1-2012

Multimodal Imaging Evidence for Axonal and Myelin Deterioration in Amnestic Mild Cognitive Impairment

Brian T. Gold
University of Kentucky, brian.gold@uky.edu

Yang Jiang
University of Kentucky, yang.jiang@uky.edu

David K. Powell
University of Kentucky, dkpowe2@uky.edu

Charles D. Smith
University of Kentucky, csmith@mri.uky.edu

Right click to open a feedback form in a new tab to let us know how this document benefits you.

Follow this and additional works at: https://uknowledge.uky.edu/neurobio_facpub

Part of the Bioimaging and Biomedical Optics Commons, Neurology Commons, and the Neuroscience and Neurobiology Commons

Multimodal Imaging Evidence for Axonal and Myelin Deterioration in Amnestic Mild Cognitive Impairment

Multimodal Imaging Evidence for Axonal and Myelin Deterioration in Amnestic Mild Cognitive Impairment

Brian T. Gold[1,3,5], **Yang Jiang**[2,3,5], **David K. Powell**[5], and **Charles D. Smith**[3,4,5]

[1]Department of Anatomy and Neurobiology, University of Kentucky, Lexington, KY, USA

[2]Department of Behavioral Sciences, University of Kentucky, Lexington, KY, USA

[3]Sanders-Brown Center on Aging, Alzheimer's Disease Center, University of Kentucky, Lexington, KY, USA

[4]Department of Neurology, University of Kentucky, Lexington, KY, USA

[5]Magnetic Resonance Imaging and Spectroscopy Center, Chandler Medical Center, University of Kentucky, Lexington, KY, USA

Abstract

White matter (WM) microstructural declines have been demonstrated in Alzheimer's disease and amnestic mild cognitive impairment (aMCI). However, the pattern of WM microstructural changes in aMCI after controlling for WM atrophy is unknown. Here, we address this issue through joint consideration of aMCI alterations in fractional anisotropy, mean diffusivity, axial diffusivity, and radial diffusivity, as well as macrostructural volume in WM and gray matter compartments. Participants were 18 individuals with aMCI and 24 healthy seniors. Voxelwise analyses of diffusion tensor imaging data was carried out using tract-based spatial statistics (TBSS) and voxelwise analyses of high-resolution structural data was conducted using voxel based morphometry. After controlling for WM atrophy, the main pattern of TBSS findings indicated reduced fractional anisotropy with only small alterations in mean diffusivity/radial diffusivity/axial diffusivity. These WM microstructural declines bordered and/or were connected to gray matter structures showing volumetric declines. However, none of the potential relationships between WM integrity and volume in connected gray matter structures was significant, and adding fractional anisotropy information improved the classificatory accuracy of aMCI compared to the use of hippocampal atrophy alone. These results suggest that WM microstructural declines provide unique information not captured by atrophy measures that may aid the magnetic resonance imaging contribution to aMCI detection.

Keywords

Alzheimer's disease; atrophy; diffusion tensor imaging; mild cognitive impairment

INTRODUCTION

Alzheimer's disease (AD) has well-established neurodegenerative effects on cerebral gray matter (GM) [1, 2]. However, there is pathological evidence that AD also affects cerebral white matter (WM) microstructure [3, 4]. The advent of magnetic resonance diffusion tensor

imaging (DTI) has made it possible to explore AD-based WM microstructural alterations *in vivo.* DTI is sensitized to the random motion of water molecules as they interact within tissues, thus reflecting characteristics of their immediate structural surroundings at a nominal 50 micron scale. Two of the most commonly used indices of WM microstructural integrity are fractional anisotropy (FA) and mean diffusivity (MD). Decreased FA is thought to reflect a reduction in axonal structure/coherence, demyelination, small vessel alterations, and degradation of microtubules [5, 6]. MD is thought to represent an overall measure of cellular integrity, with increases reflecting a loss of both neurons and glia [5, 6].

Reduced FA and/or increased MD has been observed in AD and its typical prodromal state of amnestic mild cognitive impairment (aMCI) [7], and even in cognitively normal seniors at high AD-risk [8]. However, it is unknown whether these WM microstructural declines provide unique information from measures of gross tissue atrophy in aMCI. An increased understanding in this area may be of future clinical relevance because aMCI has been shown to represent early-stage AD in the majority of cases that have come to autopsy or have been followed longitudinally to the point of transition to clinical dementia [9–11]. Increased understanding of the neurobiological bases of WM integrity declines in aMCI may help guide the development of new targets for interventions intended to slow or prevent transition to AD. In addition, if WM integrity markers provide unique biologic information distinct from that provided by measures of cerebral atrophy, then these markers may improve the diagnostic prediction of aMCI and/or conversion from aMCI to AD.

Knowledge about whether WM microstructural declines provide unique information from measures of gross tissue atrophy in aMCI would benefit from consideration of: 1) WM macrostructural atrophy; 2) GM macrostructural atrophy; and 3) the four main metrics of the diffusion tensor [FA, MD, axial diffusivity (DA), and radial diffusivity (DR)]. WM microstructural declines have been shown to be strongly correlated with WM atrophy [12, 13]. It is thus important to identify WM microstructural changes not attributable to macrostructural WM atrophy. Because WM atrophy tends to be relatively circumscribed in aMCI, it should be possible to include WM atrophy information in DTI analyses in order to identify WM microstructural changes that are not attributable to WM atrophy. To our knowledge, no aMCI studies to date have controlled for WM atrophy in DTI analyses.

After controlling for WM atrophy, information about the nature of remaining WM microstructural declines could then be gained through joint consideration of FA/MD/DR/ DA. In particular, exploring the patterns of overlap of MD/DR/DA with regions of reduced FA can provide more information about the neurobiological bases of WM integrity than the separate exploration of these metrics of the diffusion tensor [14, 15]. For example, regions showing decreased FA *and overlapping* increases in MD and/or decreases in DA are thought to reflect gross tissue loss [16], while those showing decreased FA *and overlapping* increases in DR are suggestive of reduced myelin integrity [17]. In contrast, FA reductions not solely driven by either DA or DR changes alone may reflect a subtle mixture of damage to axonal structures and the surrounding myelin sheath [15, 16].

The goals of the this study were: 1) to show whether DTI-based patterns of diffusivity can be identified that are not attributable to WM atrophy in aMCI; 2) to assess potential relationships between WM microstructural declines and GM atrophy; and 3) to determine whether the addition of WM integrity information improves the classificatory accuracy of aMCI participants compared to the classificatory accuracy achieved from using hippocampal GM alone.

MATERIALS AND METHODS

Participants

The research procedures were approved by the Institutional Review Board of the University of Kentucky Medical Center, and all participants provided informed written consent. Participants were community-dwelling individuals who were right-handed, with normal or corrected-to-normal visual acuity, and were recruited from the University of Kentucky Alzheimer's Disease Center (UK-ADC) longitudinal normal volunteer cohort. Inclusion criteria for this cohort are minimum 65 years of age, cognitive and neurological normality at enrollment, agreement to brain donation to the UK-ADC at death, a designated informant for structured interviews, and willingness to undergo annual examinations. Participants were excluded from the cohort if they had a history of substance abuse (including alcohol), major head injury (a head injury resulting in loss of consciousness for which the patient was hospitalized), major psychiatric illness (e.g., bipolar disorder, major depression, or schizophrenia), medical illnesses that are unstable (requiring other than routine follow-up and medical management) and/or have an effect on the central nervous system (e.g., encephalitis, meningitis, stroke, multiple sclerosis, epilepsy, Parkinsonism, or other neurologic disease). The annual evaluation includes a comprehensive, standardized neuropsychological battery prescribed by the NIA-Alzheimer's Disease Centers National Alzheimer's Coordinating Center Uniform Data Set (http://www.alz.washington.edu/).

Participants in the present study were 24 healthy seniors (HS) without cognitive impairment and 18 seniors with aMCI (Table 1). None of the participants had uncontrolled hypercholesterolemia, hypertension, or diabetes. The HS and aMCI groups did not differ in age [$t(34) = 0.23$, $p = 0.91$]. The two groups also did not differ in gender distribution [$\chi^2 (1) = 0.83$, $p = 0.76$] or mean number of years of education [$t(24) = 0.61$, $p = 0.86$]. All individuals receiving a diagnosis of aMCI met the following criteria: 1) a Clinical Dementia Rating (CDR) total score of 0.5, with a CDR box score of at least 0.5 for memory; 2) a documented memory complaint; and 3) a score 1.5 SD below their prior annual assessment on the Wechsler Memory Scale total memory score and Consortium to Establish a Registry for AD (CERAD) word list delayed recall. All participants in the present study were scanned within three months of their diagnosis as HS or aMCI.

Magnetic Resonance Imaging (MRI) Acquisition Procedures

Data were collected on a 3 Tesla Siemens TIM scanner at the University of Kentucky, using an 8-channel head array coil. Whole-brain diffusion tensor images (40 contiguous 3 mm thick axial slices) were acquired with 36 non-collinear encoding directions ($b = 1000$ sec/mm^2) using a double spin echo EPI sequence and the following parameters: repetition time = 6900 ms, echo time (TE) = 105 ms, flip angle = 90°, acquisition matrix = 128×128, field of view = 224 mm, in-plane resolution = 1.75×1.75 mm voxels). Five images were acquired without diffusion weighting ($b = 0$ sec/mm^2, $b0$). In addition, a double-echo gradient-echo sequence (TE1 = 5.19 ms, TE2 = 7.65 ms) with slice position and spatial resolution matching those of the EPI acquisition was used to map the spatial inhomogeneity of the B_0 field.

Whole-brain structural imaging was performed using a three-dimensional magnetization-prepared rapid gradient echo (MP-RAGE) sequence and the following parameters: repetition time = 2100 ms, TE = 2.93 ms, inversion time = 1100 ms, flip angle = 12°, field of view = 224×256×192 mm, sagittal partitions, yielding isotropic 1 mm^3 voxels.

MRI Analysis Procedures

Structural preprocessing—Preprocessing and analyses of anatomic structural images were carried out via voxel-based morphometry (VBM), using the statistical parametric mapping software package (SPM5, http://www.fil.ion.ucl.ac.uk/spm) implemented in Matlab 6.5 (Math Works, Natick, MA). Preprocessing of images included segmentation, bias correction, and spatial normalization, incorporated into a single generative model [18]. MRIs were segmented into GM, WM, and cerebrospinal fluid (CSF) images using SPM5 prior probability templates [18]. GM and WM images were normalized to their own custom templates in the standard space of the Montreal Neurological Institute (MNI) T1-weighted template using a set of non-linear basis functions. A modulation step was also incorporated into the preprocessing model in order to explore regional differences in absolute volume. Intracranial volume was estimated as the sum of GM, WM, and CSF volume for each participant (for use as a nuisance covariate in subsequent statistical analysis). As a final preprocessing step, all normalized, modulated, GM and WM images were smoothed using an 8 mm FWHM isotropic Gaussian kernel.

Structural voxelwise analysis—The preprocessed GM/WM data were analyzed within the framework of the general linear model. Statistical parametric maps of between-group (HS compared to aMCI) differences in GM/WM volume were determined using a full-factorial model (a two-sample t-test) with unequal variance and age, gender, and intracranial volume as nuisance covariates. Second-level, group linear contrasts were then conducted on parameter estimates from the model. The voxel values for the contrasts constituted a statistical parametric map (SPM) of the t statistic. Differences between groups were assessed using a statistical threshold of $p<0.05$ (family-wise error corrected for multiple comparisons).

DTI preprocessing—DTI data was pre-processed and analyzed using the Functional MRI of the Brain (FMRIB) software library (FSL v4.1.5). Raw images were pre-processed to correct for motion and residual eddy current distortion using a 12-parameter affine alignment to the corresponding $b0$ image via FMRIB's Linear Image Registration Tool (FLIRT: http://www.fmrib.ox.ac.uk/fsl). Images were then corrected for static field inhomogeneity distortions using B_0 field maps. Next, FMRIB's Diffusion Toolbox (FDT v2.0) was used to fit the diffusion tensor and calculate eigenvalues, FA, MD, DA, and DR. Registration of FA images into MNI152 space and subsequent voxelwise analyses followed a series of procedures known as Tract-Based Spatial Statistics (TBSS v1.2; http://www.fmrib.ox.ac.uk/fsl/tbss/) [19], as described in detail in our previous work [20, 21]. Briefly, all subjects' FA images were aligned to a common target using a nonlinear registration approach, and FA datasets were then affine registered and resampled to $1 \times 1 \times 1$ mm MNI152 space.

MNI-transformed FA images were then averaged to generate a mean FA image that was used to create a common WM tract skeleton. The skeleton is thinned so that it represents the center of all tracts common to the group and then thresholded at an FA value of 0.2 in order to minimize partial volume effects after warping across subjects. Each participant's aligned FA image was subsequently projected onto the FA skeleton in order to account for residual misalignments between participants after the initial nonlinear registration. Each subject's MD, DA, and DR maps in MNI space were then projected onto the common tract skeleton using the pipeline for non-FA data provided by TBSS, which employs the projection vectors from each individual's FA-to-skeleton transformation [19].

DTI voxelwise analyses—The FA/MD/DR/DA analyses included WM atrophy as a covariate to address the issue of dependence of the diffusivity effects on WM atrophy.

Voxelwise statistical analyses were performed via a permutation-based inference for nonparametric statistical thresholding using FSL's "randomize" [22]. Between group comparisons of FA/MD/DR/DA values within the tract skeleton were tested using a two-sample t-test. Nuisance covariates were age, gender, and normalized WM volume in the two regions of interest (ROIs) showing WM atrophy: the right cingulum and left temporal WM. A permutation nonparametric test (using the maximum number of 5000 permutations) was employed using a threshold-free cluster enhancement in order to avoid the use of an arbitrary threshold in the initial cluster formation. Results were then thresholded at $p < 0.05$ (corrected for multiple comparisons).

In addition to the separate analyses of FA/MD/DR/DA, to characterize the neurobiological bases of significant FA declines in the aMCI group, a second set of analyses were run in which MD, DR, and DA statistical maps were masked by regions showing significant FA reductions. Anatomical locations of significant clusters were detected using the Johns Hopkins University WM tractography atlas and the International Consortium of Brain Mapping-DTI white matter labels atlas.

Structural and DTI correlation analyses—Several criteria were considered in an attempt to focus on biologically meaningful comparisons and to maximize power to detect potential relationships between WM microstructure and GM volume. First, ROIs were centered on clusters showing GM/WM reductions in the aMCI group in the VBM/DTI voxelwise analyses. This approach is likely to provide more power than the use of *a priori* ROIs of entire tracts/gyri, which could miss potential relationships by averaging across 'intact' and 'diseased' portions of large structures. Second, because DTI voxelwise results revealed aMCI declines in FA (with minimal declines in MD, DR, or DA), correlation analyses focused on potential FA-volume relationships. Third, correlations explored potential relationships between WM tracts and GM structures with established connections based on previous work [23–25]. Based on these criteria, a total of nine correlations were between FA and GM volume. The correlations were between bilateral cinguli (CING) and their corresponding hippocampi; the left CING and left parahippocampal gyrus; bilateral uncinate fasciculi (UNC) and their corresponding hippocampi; left UNC and left parahippocampal gyrus; the splenium (SPL) and bilateral precunei; and the left superior longitudinal fasciculus (SLF) and left lateral parietal cortex.

For both volumetric and FA data, ROI masks consisted of a three-dimensional area including all contiguous voxels showing significance in the HS > aMCI voxelwise statistical map. Structural volumetric (GM and WM) ROI masks were generated using the WFU Pickatlas [26]. Volumetric ROI masks were applied to each subject's smoothed, normalized, modulated GM/WM images, and ROI-masked volumes (the sum of the voxels' intensities within that ROI multiplied by voxel volume) were then computed for each subject. All volumetric ROI volumes were 'normalized' (divided by intracranial volume), providing an estimate of atrophy in that ROI. Diffusion (FA) ROI masks were created from significant clusters using FSL's 'fslmaths'. Masks were then applied to each subject's FA images using FSL's 'fslmeants' to extract mean FA in that ROI.

Receiver Operating Characteristic Analyses

Receiver operating characteristic (ROC) curves were generated from logistic regression models with group (aMCI versus HS) as the dependent variable by calculating the area under the curve (AUC). Model 1 explored the classificatory accuracy of mean FA across bilateral posterior CING. Model 2 explored the classificatory accuracy of mean normalized volumes across bilateral hippocampi. Model 3 explored the classificatory accuracy of the combination of models 1 and 2.

RESULTS

Voxel-Based Morphometry

Figure 1 presents the results from the group comparisons of WM and GM volume. The aMCI group showed WM volumetric reductions in the right CING and left temporal lobe (panel A). GM volumetric reductions were observed in bilateral portions of the hippocampal complex, left parahippocampal gyrus, bilateral portions of the precuneus, and left lateral parietal cortex (panels B and C). The largest cluster of reduced GM volume in the aMCI group was primarily located in the left precuneus, although its peak effect was within the right precuneus (4 –56 16; 107 voxels).

White Matter Microstructural Integrity

Figure 2 presents the results from the group comparisons of FA and MD after controlling for WM atrophy. The anatomic underlay is the MNI152 standard brain. The aMCI group showed decreased FA (shown in red) compared to the HS group in a number of regions, prominently including portions of the CING, the SPL, and SLF in the parietal lobes; portions of the inferior longitudinal fasciculus (ILF) in the temporal lobe; and portions of the UNC in the frontal lobe. Within these regions of decreased FA, there was only one region of increased MD in the aMCI group (shown in orange): an anterior portion of the CING. There were no regions in which the HS group showed decreased FA or increased MD compared to the aMCI group.

Figure 3 (top panel) presents the results from the comparison of component diffusivities (DR and DA) that overlap with regions showing lower FA in the aMCI group. There were only a few regions in which FA declines in the aMCI group were driven solely by DR or DA. Regions of decreased FA showing increased DR in the aMCI group (shown in blue) were portions of the anterior limb of the internal capsule and the CING. Regions of decreased FA showing decreased DA in the aMCI group (shown in yellow) were restricted to small portions of the corticospinal tracts. Finally, there were no regions in which the aMCI group showed increased DA.

Figure 3 (bottom panel) presents the results from the voxelwise comparison of DR and DA that did not overlap with regions showing lower FA in the aMCI group. There were only a few regions showing altered component diffusivities in the aMCI group. Regions showing increased DR were small portions of the CING, UNC, and ILF. Regions showing decreased DA in the aMCI group were portions of the corticospinal tracts and the SLF. There were no regions in which the aMCI group showed increased DA.

Correlation Analyses

Regression scattergrams of FA versus GM volume are presented in Figure 4. None of the nine potential relationships was significant at a family-wise significance threshold of $p < 0.006$ (0.05 divided by 9 comparisons). Even when a liberal significance threshold of $p < 0.05$ (uncorrected) was employed, only one out of nine potential relationships was significant: FA in the SPL and volume in the left precuneus [$F = 5.1$, $p = 0.038$]. In contrast, there was no relationship between FA in the SPL and volume in the right precuneus [$F = 0.69$ $p = 0.42$]. There was no relationship between FA in the left SLF and volume in the left lateral parietal region [$F = 0.93$ $p = 0.35$]. There were no relationships between FA in the left/right CING and volume in the left/right hippocampi (both p's 0.39). There were no relationships between FA in the left/right UNC and volume in the left/right hippocampi (both p's 0.36). There were no relationships between FA in the left CING or left UNC and volume in the left parahippocampal gyrus (both p's 0.78).

In contrast, and as expected, the two potential relationships between FA and WM volume were significant at a family-wise significance threshold of p < 0.025 (0.05 divided by 2 comparisons). FA in the right CING and volume in the right CING were significantly correlated [r (16) = 0.65, p = 0.003]. In addition, FA in the left temporal lobe ROI and volume in the left UNC were significantly correlated [r (16) = 0. 59, p = 0.009].

Receiver Operating Characteristic Analyses

The AUC for the models of each measure is presented in Figure 5. The AUC was 0.75 for the model of mean FA in bilateral CING. The AUC was 0.77 for the model of mean normalized volume in bilateral hippocampi. When FA in the CING and volume in the hippocampi were combined into a single model, discriminatory accuracy increased to 0.91.

DISCUSSION

There were three main findings of the present study related to the nature of WM microstructural declines in aMCI. First, WM microstructural changes not attributable to WM atrophy were characterized primarily by reduced FA, with smaller changes in MD and component diffusivities (DR/DA). Second, reductions in the microstructural integrity of WM tracts were relatively independent from atrophy in connected GM structures. Third, FA was found to provide unique information compared to GM atrophy in discriminating aMCI from HS. Classification accuracy in this study increased from AUC 0.77 using hippocampal volume alone to 0.91 when CING FA was added to this volumetric GM information. The details of these findings are discussed below.

The VBM analysis demonstrated WM atrophy in the right CING and left temporal lobe. The relatively circumscribed WM atrophy in aMCI is consistent with previous reports, although atrophy in portions of the corpus callosum has also been observed in previous aMCI studies [27–28]. As expected, WM volumetric declines were correlated and FA declines in the right CING and left temporal lobe. WM volumetric declines were thus included as nuisance covariates in DTI analyses to identify WM integrity changes not detectable with conventional volumetric MRI. GM volumetric reductions were more extensive than WM volumetric declines. Specifically, GM atrophy was observed in bilateral hippocampi, left parahippocampal gyrus, bilateral precunei, and left lateral parietal cortex, consistent with previous reports of medial temporal and parietal GM atrophy in aMCI [29–31]. However, unlike WM atrophy, GM reductions were not correlated with FA declines (discussed below).

After controlling for WM atrophy, joint consideration of the major components of the diffusion tensor revealed several patterns of WM integrity changes in the aMCI group. A predominant pattern was reduced FA in the absence of differences in MD, DA, or DR. Regions showing decreased FA in the aMCI group in the absence of alterations in MD, DA, or DR included portions of the CING, UNC, SPL, ILF, and SLF. In contrast, only a few WM tracts showing decreased FA in the aMCI group showed overlapping alterations in MD, DA, or DR. We also explored the possibility of altered component diffusivities in the aMCI group outside of regions of decreased FA. Once again, only a few WM tracts showed alterations in component diffusivity. Taken together, this pattern of diffusivity results suggest that WM integrity changes in aMCI reflect a subtle mixture of axonal and myelin damage, possibly resulting from minor loss of fibers and their surrounding myelin sheath [15,16].

Many of the GM regions showing atrophy were those bordering and/or connected to WM tracts showing microstructural declines. For example, the medial temporal lobe regions showing atrophy (hippocampus and parahippocampal gyrus) connect to the posterior cingulate cortex via caudal portions of the CING [23], which showed reduced WM integrity

in the present results. However, none of the nine potential relationships between WM integrity and volume in connected GM structures was significant when controlling for multiple comparisons. Even when a more liberal significance threshold of $p < 0.05$ (uncorrected) was employed, only one out of nine potential relationships was significant. This pattern of weak correlations was observed despite the attempt to maximize power for this analysis by centering ROIs on clusters showing peak WM/GM reductions in the aMCI group in the voxelwise analyses.

In the other eight potential GM volume-FA relationships tested, correlations were weak (r's between $0.11 – 0.28$) and did not even approach an uncorrected significance threshold. In addition, there were no increases in MD or DA in these WM tracts. These data are inconsistent with a view that WM integrity tract reductions are merely a secondary consequence of GM degeneration in aMCI. Our results in aMCI contrast with those in AD, where positive correlations between FA/MD and GM volume have been reported [32–36]. Relatively less is known about the relationship between WM integrity reductions and GM atrophy in aMCI, with some recent studies reporting a relationship and others reporting no relationship [34, 37, 38]. There are several possible reasons for the different correlation results observed in the present aMCI study and previous AD studies. One possibility is that GM atrophy and WM integrity reductions may be differentially sensitive to classic AD pathological features (i.e., amyloid plaques and neurofibrillary tangles) early in the disease process. A second possibility is that classic AD pathologies may progress at different rates within cerebral GM and WM. A third possibility is that DTI declines in aMCI reflect other as yet unknown pathologies more specifically related to WM. Future studies should test between these possibilities by correlating FA with AD-related CSF analytes such as $A\beta_{1–42}$ and phosphorylated tau (P-tau$_{181}$), as well as with other analytes reflecting the integrity of myelin (e.g., myelin basic protein), inflammatory mediators, and protein/protein complexes. In addition, future studies should explore the cerebral biochemical correlates of WM integrity changes in early AD states through correlations between FA declines and MR spectroscopy measures of metabolite ratios reflecting various molecular and cellular processes.

Results from ROC classification analyses suggest that combining WM integrity and GM atrophy information improves classification of aMCI. The model that explored FA in bilateral CING ROIs differentiated the aMCI and HS groups with 75% accuracy, which was similar to the accuracy of 77% achieved for the model which explored structural volumes in bilateral hippocampi. However, when DTI and volumetric parietal ROIs were combined into a single model, discriminatory accuracy increased to 91%. This finding complements our correlation results, again suggesting that WM integrity reductions and atrophy in connected structures provide complementary rather than redundant information in aMCI. However, we interpret the high classificatory accuracy of the combined DTI-volumetric model cautiously because our study was cross-sectional and had a relatively small sample size. Future research will be required to determine the predictive accuracy of similar combined WM integrity/GM atrophy models in predicting conversion from aMCI to AD.

We note several caveats of the present study. First, the cross-sectional design does not allow for assessment of the relative timing of GM atrophy and WM integrity declines. Second, correlation analyses focused on FA because minimal alterations were observed in other diffusivity measures, limiting power for potential correlations between these measures and GM volume. Future studies will be required to assess potential relationships between MD/DR/DA and volumetric reductions in connected structures. Third, as with all cross-sectional studies of aMCI, we are not yet able to confirm that all aMCI participants will develop AD. It should be noted that subtle impairment in executive function, as observed in the present aMCI group, have been reported even in pure aMCI and tend to be predictive of future AD

[39]. In addition, most individuals with a clinical diagnosis of aMCI at our center show AD pathology [40]. Nevertheless, it is not yet possible to know what percentage of the present aMCI or normal samples harbor significant AD pathology. This issue should be addressable in the future because participants in the longitudinal normal cohort study at our ADRC have agreed to brain donation at death.

In conclusion, our results identify WM microstructural declines in aMCI that cannot be appreciated by conventional measures of WM atrophy. In general, FA declines were characterized by a pattern of decreased DA and increased DR (rather than more selective changes in one component diffusivity), suggesting reductions in both axonal and myelin integrity in aMCI. The lack of correlation between WM microstructural declines and atrophy in connected GM structures justifies future research intended to understand the relationship between WM integrity and CSF analytes representing classic AD pathology and other pathologies which may be more specifically related to WM. Finally, adding WM integrity information to classic AD medial temporal lobe atrophy models may improve prediction of AD and this issue should be explored in future longitudinal studies.

Acknowledgments

References

1. Braak H, Braak E. Neuropathological stageing of Alzheimer-related changes. Acta Neuropathol. 1991; 82:239–259. [PubMed: 1759558]

2. Hyman BT, Van Hoesen GW, Damasio AR, Barnes CL. Alzheimer's disease: cell-specific pathology isolates the hippocampal formation. Science. 1984; 225:1168–1170. [PubMed: 6474172]

3. Brun A, Englund E. A white matter disorder in dementia of the Alzheimer type: a pathoanatomical study. Ann Neurol. 1986; 19:253–262. [PubMed: 3963770]

4. Englund E, Brun A, Alling C. White matter changes in dementia of Alzheimer's type. Biochemical and neuropathological correlates. Brain. 1988; 111 (Pt 6):1425–1439. [PubMed: 3208064]

5. Bronge L, Bogdanovic N, Wahlund LO. Postmortem MRI and histopathology of white matter changes in Alzheimer brains. A quantitative, comparative study. Dement Geriatr Cogn Disord. 2002; 13:205–212. [PubMed: 12006730]

6. Moseley M. Diffusion tensor imaging and aging - a review. NMR Biomed. 2002; 15:553–560. [PubMed: 12489101]

7. Stebbins GT, Murphy CM. Diffusion tensor imaging in Alzheimer's disease and mild cognitive impairment. Behav Neurol. 2009; 21:39–49. [PubMed: 19847044]

8. Gold BT, Johnson NF, Powell DK, Smith CD. White matter integrity and vulnerability to Alzheimer's disease: Preliminary findings and future directions. Biochim Biophys Acta. 2012; 1822:416–422. [PubMed: 21803153]

9. Jicha GA, Parisi JE, Dickson DW, Johnson K, Cha R, Ivnik RJ, Tangalos EG, Boeve BF, Knopman DS, Braak H, Petersen RC. Neuropathologic outcome of mild cognitive impairment following progression to clinical dementia. Arch Neurol. 2006; 63:674–681. [PubMed: 16682537]

10. Markesbery WR, Schmitt FA, Kryscio RJ, Davis DG, Smith CD, Wekstein DR. Neuropathologic substrate of mild cognitive impairment. Arch Neurol. 2006; 63:38–46. [PubMed: 16401735]

11. Morris JC, Storandt M, Miller JP, McKeel DW, Price JL, Rubin EH, Berg L. Mild cognitive impairment represents early-stage Alzheimer disease. Arch Neurol. 2001; 58:397–405. [PubMed: 11255443]

12. Salat DH, Tuch DS, Hevelone ND, Fischl B, Corkin S, Rosas HD, Dale AM. Age-related changes in prefrontal white matter measured by diffusion tensor imaging. Ann N Y Acad Sci. 2005; 1064:37–49. [PubMed: 16394146]

13. Hugenschmidt CE, Peiffer AM, Kraft RA, Casanova R, Deibler AR, Burdette JH, Maldjian JA, Laurienti PJ. Relating imaging indices of white matter integrity and volume in healthy older adults. Cereb Cortex. 2008; 18:433–442. [PubMed: 17575289]

14. Assaf Y, Pasternak O. Diffusion tensor imaging (DTI)-based white matter mapping in brain research: a review. J Mol Neurosci. 2008; 34:51–61. [PubMed: 18157658]

15. Burzynska AZ, Preuschhof C, Backman L, Nyberg L, Li SC, Lindenberger U, Heekeren HR. Age-related differences in white matter microstructure: region-specific patterns of diffusivity. Neuroimage. 2010; 49:2104–2112. [PubMed: 19782758]

16. Sen PN, Basser PJ. A model for diffusion in white matter in the brain. Biophys J. 2005; 89:2927–2938. [PubMed: 16100258]

17. Ciccarelli O, Behrens TE, Altmann DR, Orrell RW, Howard RS, Johansen-Berg H, Miller DH, Matthews PM, Thompson AJ. Probabilistic diffusion tractography: a potential tool to assess the rate of disease progression in amyotrophic lateral sclerosis. Brain. 2006; 129:1859–1871. [PubMed: 16672290]

18. Ashburner J, Friston KJ. Unified segmentation. Neuroimage. 2005; 26:839–851. [PubMed: 15955494]

19. Smith SM, Jenkinson M, Johansen-Berg H, Rueckert D, Nichols TE, Mackay CE, Watkins KE, Ciccarelli O, Cader MZ, Matthews PM, Behrens TE. Tract-based spatial statistics: voxelwise analysis of multi-subject diffusion data. Neuroimage. 2006; 31:1487–1505. [PubMed: 16624579]

20. Smith CD, Chebrolu H, Andersen AH, Powell DA, Lovell MA, Xiong S, Gold BT. White matter diffusion alterations in normal women at risk of Alzheimer's disease. Neurobiol Aging. 2010; 31:1122–1131. [PubMed: 18801597]

21. Gold BT, Powell DK, Andersen AH, Smith CD. Alterations in multiple measures of white matter integrity in normal women at high risk for Alzheimer's disease. Neuroimage. 2010; 52:1487–1494. [PubMed: 20493952]

22. Nichols TE, Holmes AP. Nonparametric permutation tests for functional neuroimaging: a primer with examples. Hum Brain Mapp. 2002; 15:1–25. [PubMed: 11747097]

23. Mufson EJ, Pandya DN. Some observations on the course and composition of the cingulum bundle in the rhesus monkey. J Comp Neurol. 1984; 225:31–43. [PubMed: 6725639]

24. Kier EL, Staib LH, Davis LM, Bronen RA. MR imaging of the temporal stem: anatomic dissection tractography of the uncinate fasciculus, inferior occipitofrontal fasciculus, and Meyer's loop of the optic radiation. AJNR Am J Neuroradiol. 2004; 25:677–691. [PubMed: 15140705]

25. Catani M, Howard RJ, Pajevic S, Jones DK. Virtual in vivo interactive dissection of white matter fasciculi in the human brain. Neuroimage. 2002; 17:77–94. [PubMed: 12482069]

26. Maldjian JA, Laurienti PJ, Kraft RA, Burdette JH. An automated method for neuroanatomic and cytoarchitectonic atlas-based interrogation of fMRI data sets. Neuroimage. 2003; 19:1233–1239. [PubMed: 12880848]

27. Wang PJ, Saykin AJ, Flashman LA, Wishart HA, Rabin LA, Santulli RB, McHugh TL, MacDonald JW, Mamourian AC. Regionally specific atrophy of the corpus callosum in AD, MCI and cognitive complaints. Neurobiol Aging. 2006; 27:1613–1617. [PubMed: 16271806]

28. Di Paola M, Di Iulio F, Cherubini A, Blundo C, Casini AR, Sancesario G, Passafiume D, Caltagirone C, Spalletta G. When, where, and how the corpus callosum changes in MCI and AD: a multimodal MRI study. Neurology. 74:1136–1142. [PubMed: 20368633]

29. Chetelat G, Desgranges B, de la Sayette V, Viader F, Eustache F, Baron JC. Mapping gray matter loss with voxel-based morphometry in mild cognitive impairment. Neuroreport. 2002; 13:1939–1943. [PubMed: 12395096]

30. Hamalainen A, Tervo S, Grau-Olivares M, Niskanen E, Pennanen C, Huuskonen J, Kivipelto M, Haenninen T, Tapiola M, Vanhanen M, Hallikainen M, Helkala EL, Nissinen A, Vanninen R, Soininen H. Voxel-based morphometry to detect brain atrophy in progressive mild cognitive impairment. Neuroimage. 2007; 37:1122–1131. [PubMed: 17683950]

31. Karas GB, Scheltens P, Rombouts SARB, Visser PJ, van Schijndel RA, Fox NC, Barkhof F. Global and local gray matter loss in mild cognitive impairment and Alzheimer's disease. Neuroimage. 2004; 23:708–716. [PubMed: 15488420]

32. Villain N, Desgranges B, Viader F, de la Sayette V, Mezenge F, Landeau B, Baron JC, Eustache F, Chetelat G. Relationships between hippocampal atrophy, white matter disruption, and gray matter hypometabolism in Alzheimer's disease. J Neurosci. 2008; 28:6174–6181. [PubMed: 18550759]

33. Xie S, Xiao JX, Wang YH, Wu HK, Gong GL, Jiang XX. Evaluation of bilateral cingulum with tractography in patients with Alzheimer's disease. Neuroreport. 2005; 16:1275–1278. [PubMed: 16056124]

34. Agosta F, Pievani M, Sala S, Geroldi C, Galluzzi S, Frisoni GB, Filippi M. White matter damage in Alzheimer disease and its relationship to gray matter atrophy. Radiology. 2011; 258:853–863. [PubMed: 21177393]

35. Johnson DK, Barrow W, Anderson R, Harsha A, Honea R, Brooks WM, Burns JM. Diagnostic utility of cerebral white matter integrity in early Alzheimer's disease. Int J Neurosci. 2010; 120:544–550. [PubMed: 20615058]

36. Sydykova D, Stahl R, Dietrich O, Ewers M, Reiser MF, Schoenberg SO, Moller HJ, Hampel H, Teipel SJ. Fiber connections between the cerebral cortex and the corpus callosum in Alzheimer's disease: a diffusion tensor imaging and voxel-based morphometry study. Cereb Cortex. 2007; 17:2276–2282. [PubMed: 17164468]

37. Palesi F, Vitali P, Chiarati P, Castellazzi G, Caverzasi E, Pichiecchio A, Colli-Tibaldi E, D'Amore F, D'Errico I, Sinforiani E, Bastianello S. DTI and MR volumetry of hippocampus-PC/PCC circuit: in search of early micro- and macrostructural signs of Alzheimer's disease. Neurol Res Int. 2012; 2012:517876. [PubMed: 21773026]

38. Wang L, Goldstein FC, Veledar E, Levey AI, Lah JJ, Meltzer CC, Holder CA, Mao H. Alterations in cortical thickness and white matter integrity in mild cognitive impairment measured by whole-brain cortical thickness mapping and diffusion tensor imaging. AJNR Am J Neuroradiol. 2009; 30:893–899. [PubMed: 19279272]

39. Brandt J, Aretouli E, Neijstrom E, Samek J, Manning K, Albert MS, Bandeen-Roche K. Selectivity of executive function deficits in mild cognitive impairment. Neuropsychology. 2009; 23:607–618. [PubMed: 19702414]

40. Markesbery WR, Schmitt FA, Kryscio RJ, Davis DG, Smith CD, Wekstein DR. Neuropathologic substrate of mild cognitive impairment. Arch Neurol. 2006; 63:38–46. [PubMed: 16401735]
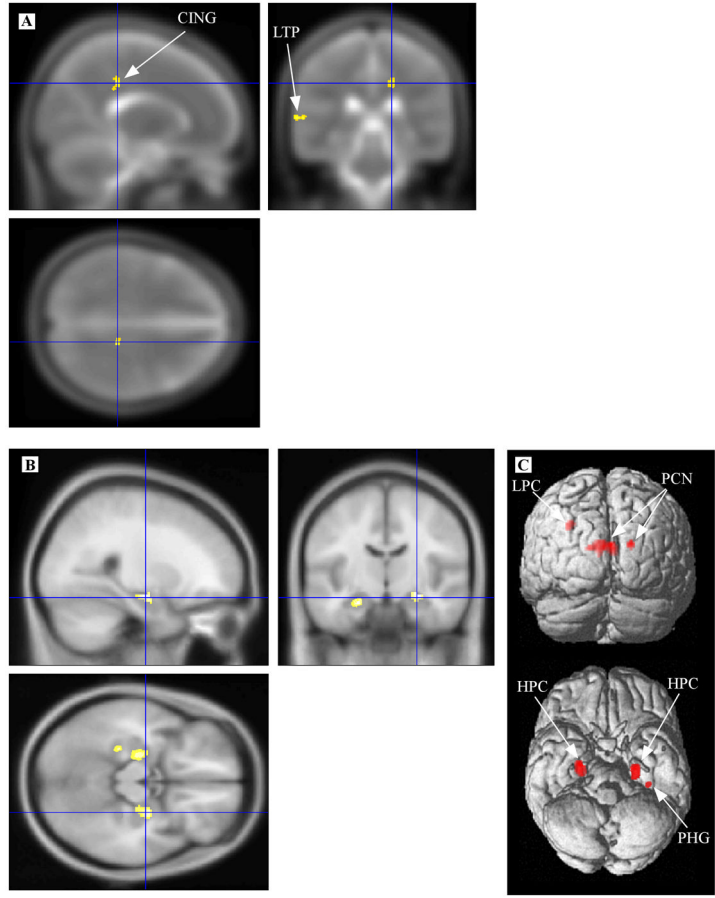
Figure 1.
Volumetric reductions in aMCI. Regions of significantly smaller volume in the aMCI group compared to the HS group are displayed after controlling for global intracranial differences. A) WM volumetric differences highlighting a cluster in the right cingulum (crosshair) are displayed on the canonical MNI T2 template. B) GM volumetric differences highlighting a cluster within the right hippocampus (crosshair) are displayed on the canonical MNI T1 template. C) The full set of GM volumetric differences are displayed on SPM's single subject, 3D rendered surface. Note: CING, cingulum; LTP, left temporal; LPC, left parietal cortex; PCN, precuneus; HPC, hippocampal complex; PHG, parahippocampal gyrus.
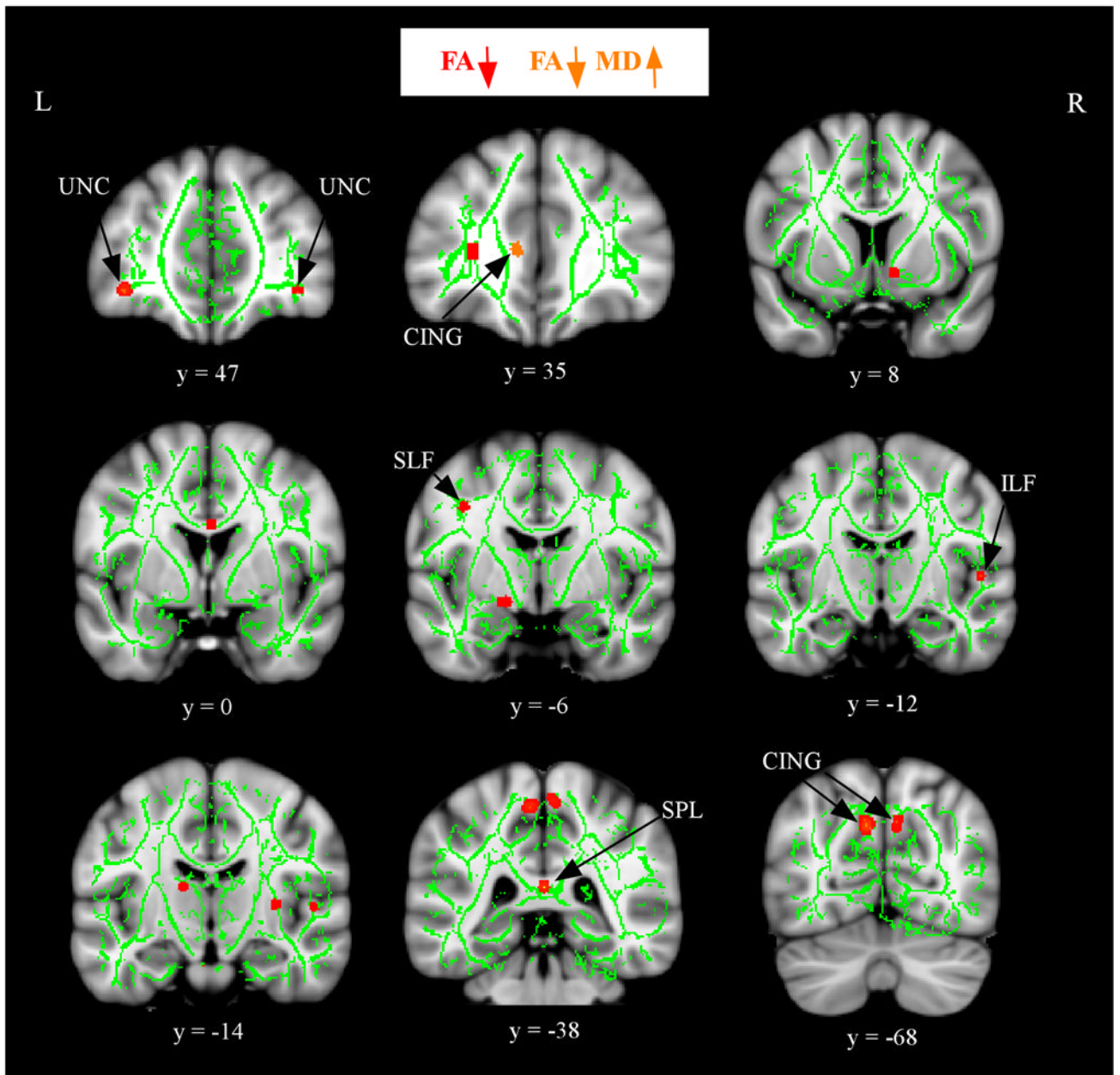
Figure 2.
Alterations in FA and MD in aMCI after controlling for WM atrophy. The anatomic underlay used for illustration is the MNI152 T1-weighted 1mm brain. The registered average FA skeleton is represented in green. Regions of decreased FA in the aMCI group are displayed in red. Regions of increased MD that overlap decreased FA in the aMCI group are displayed in orange. The numbers below coronal sections represent y coordinates in MNI space. Note: CING, cingulum; UNC, uncinate fasciculus; SLF, superior longitudinal fasciculus; ILF, inferior longitudinal fasciculus; SPL, splenium.
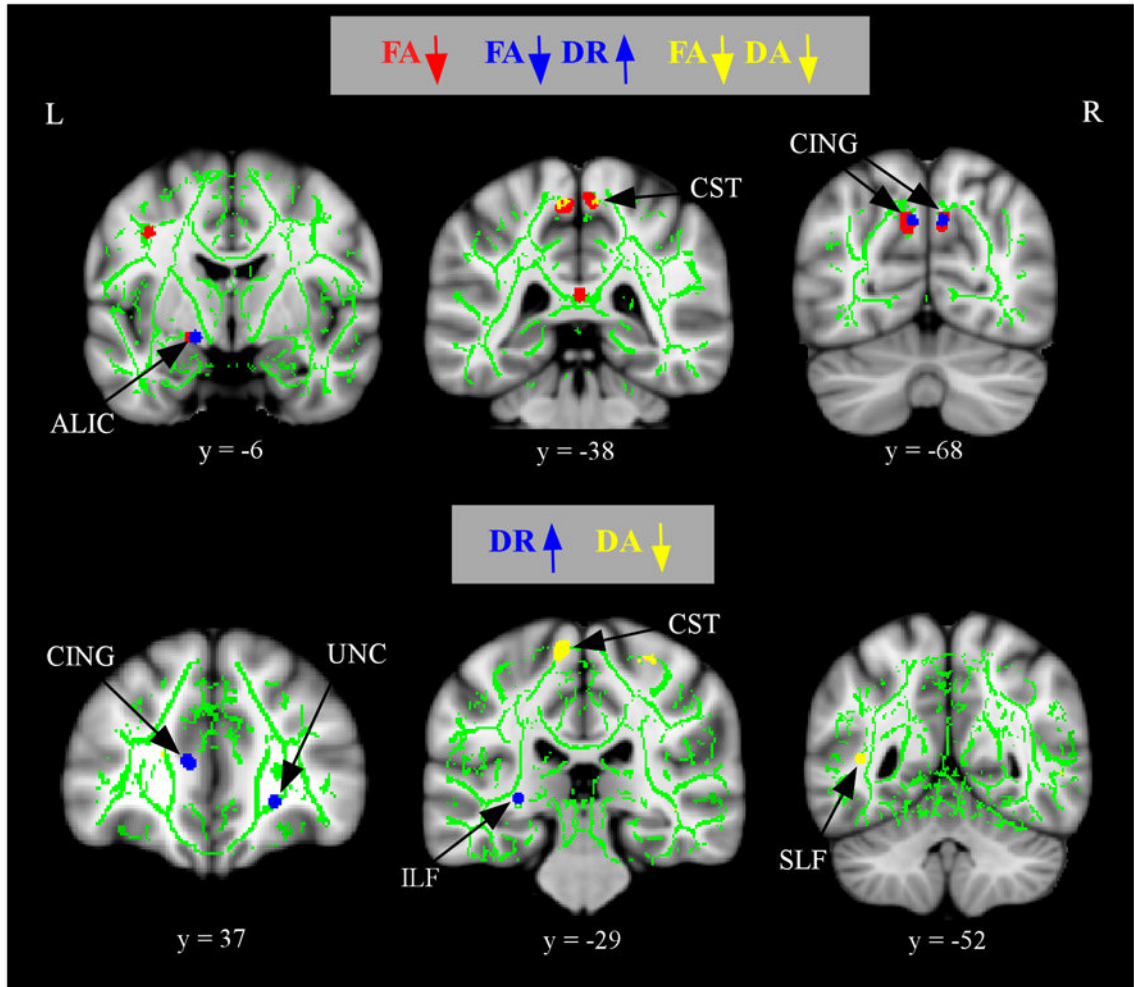
Figure 3.
Alterations in component diffusivities in aMCI after controlling for WM atrophy. The anatomic underlay and registered average FA skeleton are described in the Figure 1 legend. The top panel displays regions of increased in DR (blue) or decreased in DA (yellow) that overlap with regions of decreased FA (red) in the aMCI group. The bottom panel displays regions of increased DR (blue) or decreases in DA (yellow) that do not overlap with regions of decreased FA in the aMCI group. The numbers below coronal sections represent y coordinates in MNI space. Note: ALIC, anterior limb of the internal capsule; CING, cingulum; CST, corticospinal tracts; UNC, uncinate fasciculus; SLF, superior longitudinal fasciculus; ILF, inferior longitudinal fasciculus.
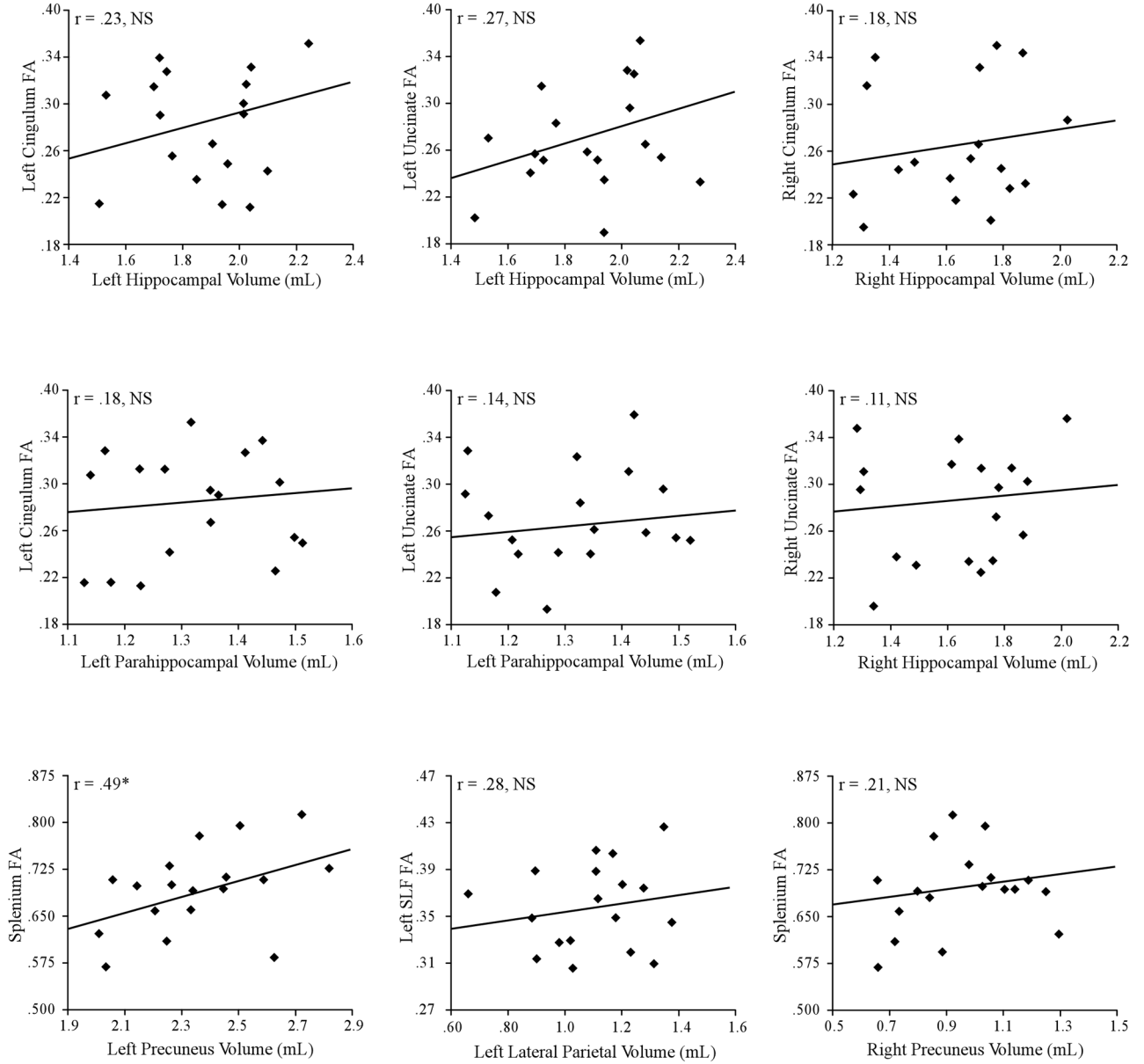
Figure 4.
The relationship between WM integrity and GM atrophy in aMCI. Regression plots display FA against normalized GM volume in nine regions. Each diamond represents one of the 18 MCI participants. *Significant at p < 0.05, uncorrected.
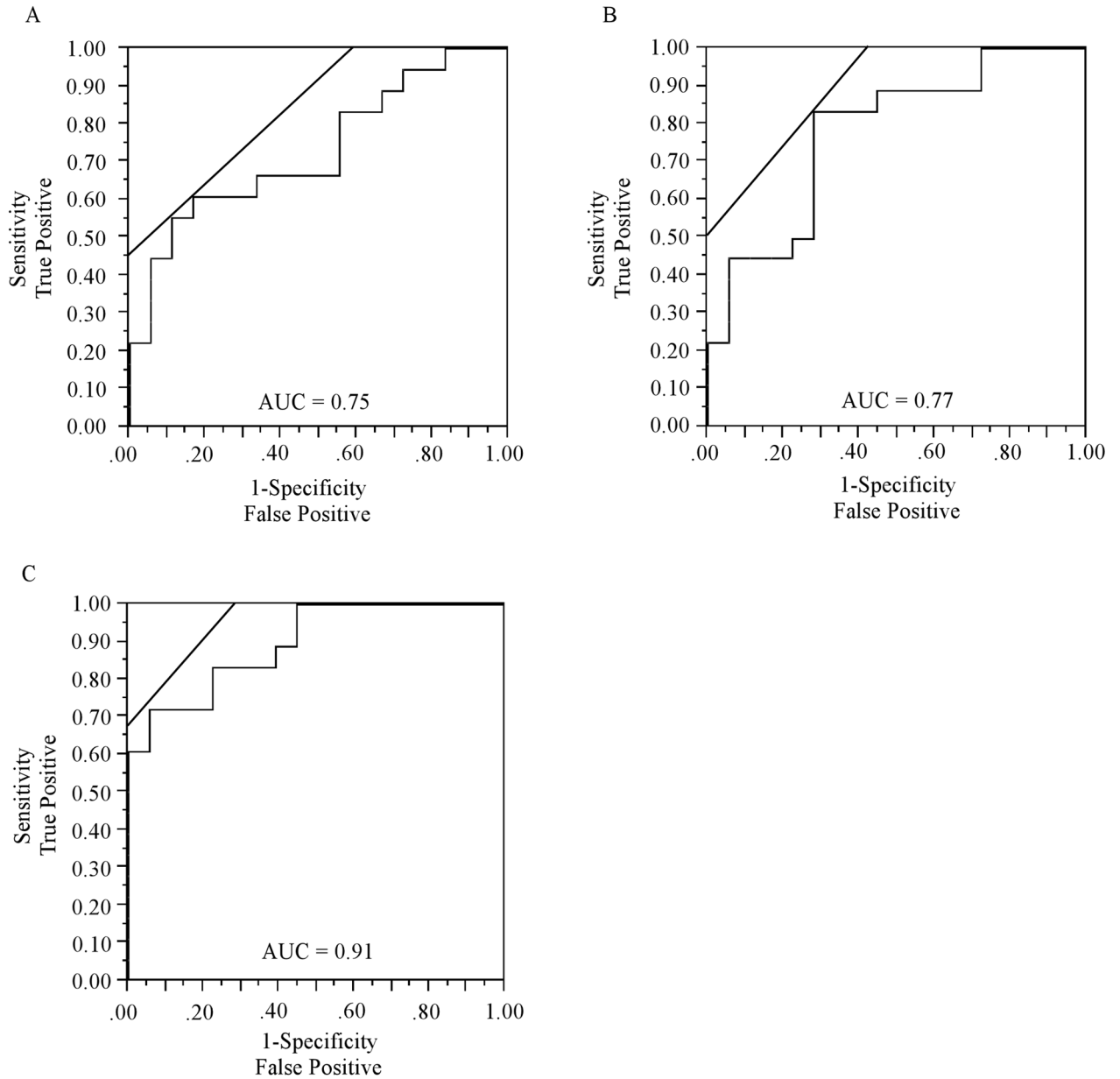
A

B

C

Figure 5.
Receiver operator characteristic (ROC) curves. ROC curves plot the sensitivity on the y-axis against 1-specificity on the x-axis. Lines at 45 degree angles tangent to the ROC curve mark the best cutoff point under the assumption that false negatives and false positives have similar costs. The ROC curves correspond to models of (A) mean FA across bilateral CING, (B) mean normalized GM volume across bilateral hippocampi, (C) a combined FA and volumetric model. The highest classificatory accuracy was obtained for the combined FA and volumetric model (AUC = 0.91).

Table 1

Subject demographics and neuropsychological scores.

	aMCI		HS	
	Mean	**S.D.**	**Mean**	**S.D.**
Age	77.1	5.8	77.9	7.1
Education	15.83	2.6	16.21	2.4
Gender	8 m/10 f		11 m/13 f	
Clinical Dementia Rating	0.5		0	
Mini Mental State Exam	27.1[*]	1.3	28.4	1.1
Wechsler Memory Scale	24.8[*]	5.9	31.6	6.2
CERAD Word list delayed	4.9[*]	2.5	6.9	1.4
Digit Span Forward	4.9	1.1	5.3	1.3
Digit Span Backward	4.1	1.3	4.4	1.6
Digit Symbol	58.6	12.4	51.4	11.8
Trails A	49.6	16.7	41.3	15.7
Trails B	109.3[*]	39.2	91.2	26.6
Boston Naming Test	23.2	2.9	25.3	3.1
Geriatric Depression Scale total score	1.6	2.3	1.4	1.1
Functional Activities Questionnaire total score	2.1	2.2	1.1	1.4

[*]
p < 0.05 statistical significance between the amnestic mild cognitive impairment (aMCI) and healthy senior (HS) groups.